Multiple Conformations of Catalytic Serine and Histidine in Acetylxylan Esterase at 0.90 Å*

Debashis Ghosh‡§¶, Mark Sawicki§‖, Puloma Lala‡§, Mary Erman‡, Walter Pangborn‡, Jaime Eyzaguirre, Rodrigo Gutiérrez**‡‡, Hans Jörnvall§§, and Daniel J. Thiel¶¶**

*From the ‡Hauptman-Woodward Medical Research Institute, Buffalo, New York 14203, the §Roswell-Park Cancer Institute, Buffalo, New York 14263, the **Pontificia Universidad Catolica de Chile, Santiago, Chile, the §§Karolinska Institutet, Stockholm SE-17177, Sweden, and the ¶¶Cornell High Energy Synchrotron Source, Ithaca, New York 14853*

Acetylxylan esterase (AXEII; 207 amino acids) from *Penicillium purpurogenum* has substrate specificities toward acetate esters of D-xylopyranose residues in xylan and belongs to a new class of α/β hydrolases. The crystal structure of AXEII has been determined by single isomorphous replacement and anomalous scattering, and refined at 0.90- and 1.10-Å resolutions with data collected at 85 K and 295 K, respectively. The tertiary structure consists of a doubly wound α/β sandwich, having a central six-stranded parallel β-sheet flanked by two parallel α-helices on each side. The catalytic residues Ser[90], His[187], and Asp[175] are located at the C-terminal end of the sheet, an exposed region of the molecule. The serine and histidine side chains in the 295 K structure show the frequently observed conformations in which Ser[90] is *trans* and the hydroxyl group is in the plane of the imidazole ring of His[187]. However, the structure at 85 K displays an additional conformation in which Ser[90] side-chain hydroxyl is away from the plane of the imidazole ring of His[187]. The His[187] side chain forms a hydrogen bond with a sulfate ion and adopts an altered conformation. The only other known hydrolase that has a similar tertiary structure is *Fusarium solani* cutinase. The exposed nature of the catalytic triad suggests that AXEII is a pure esterase, *i.e.* an α/β hydrolase with specificity for nonlipidic polar substrates.

Plant cell wall hemicelluloses are complex mixtures of heteropolysaccharides. Their main component is xylan, which is composed of a linear chain of β(1→4)glycosidic-linked D-xylopyranoses, having various substitutions at carbon 2 and 3 positions (1). Biodegradation of xylan is a complex process catalyzed by several fungal and bacterial enzymes (2). Although the linear chain is cleaved by endoxylanases and β-xylosidases,

acetylxylan esterases (AXE)[1] hydrolyze *O*-acetyl substitutions of D-xylopyranose moieties. *Penicillium purpurogenum* secretes at least two forms of AXEs, I and II, that demonstrate substrate specificities toward acetate esters of D-xylopyranose and belong to a new class of α/β hydrolases (3).

Purification and characterization of AXEs from other xylanolytic microorganisms have been described previously (4, 5). Although considerable amounts of work have been performed on the enzymology of xylanases and AXEs (6–10), the structure-function characterization of this new class of esterases with regard to their catalytic activities and substrate specificities is yet to be carried out. We reported the crystallization and structure determination using the room temperature data of the first member of the family, *P. purpurogenum* AXEII (11–13). Recently, crystallization and preliminary diffraction studies of the catalytic core of *Trichoderma reesei* AXE have been published (14). Here we present for the first time the complete description of the three-dimensional structure of *P. purpurogenum* AXEII and its active site at 0.90-Å resolution and 85 K, compare it with the 1.10-Å structure (Protein Data Bank Code: 1BS9) determined at 295 K (room temperature), and investigate the structural basis for its acetyl D-xylopyranose specificity.

MATERIALS AND METHODS

Crystallization and Data Collection—The enzyme was crystallized from ammonium sulfate solution in 50 mM citrate buffer at pH 5.3 (11). Diffraction data were collected at the A-1 station of Cornell High Energy Synchrotron Source using a 2000 × 2000 pixel charge-coupled device detector. The crystal (0.5 mm × 0.6 mm × 0.1 mm) was flash-frozen in a stream of liquid nitrogen vapor using a mixture of glycerol and polyethylene glycol as the cryoprotectant. The x-ray beam was tuned to the wavelength 0.920 Å. The entire data collection was carried out in two separate modes, a high (better than 1.6 Å) and a low resolution. A total of 403 frames of data were collected from two crystals, yielding 420,882 observations and 95,343 unique reflections between 99.0- and 0.90-Å resolution, an 86.6% complete set in the resolution range. The intensities were measured and processed with DENZO software package (15). Table I gives a summary of the results from the diffraction experiment.

Structure Solution and Refinement—Details of structure determination were previously described (12). Briefly, the crystal structure of AXEII was determined by the single isomorphous replacement and anomalous scattering (SIRAS) method using an iodine derivative. A complete atomic model of the protein was built into this SIRAS map. This starting model was refined separately with both the 1.10-Å and the 0.90-Å data sets collected at 295 K and 85 K, respectively. The refinements were carried out first with XPLOR (16) and then with SHELX97 (17), implemented on a Silicon Graphics Indigo2 workstation. We describe here the procedure carried out with the cryogenic data. The initial XPLOR refinement was conducted using a 2.0σ cut off on structure amplitudes between 99.0 and 0.90 Å, which included 94,055 reflections. The refinement process consisted of 500 cycles of positional re-

‖ Present address: Center for Advanced Research in Biotechnology, Rockville, MD 20850.

‡‡ Present Address: Department of Biochemistry, Michigan State University, E. Lansing, MI 48825.

¶ To whom correspondence should be addressed: Hauptman-Woodward Medical Research Institute, 73 High St., Buffalo, NY 14203-1196. Tel.: 716-856-9600 (ext. 316); Fax: 716-852-6086; E-mail: ghosh@hwi.buffalo.edu.

[1] The abbreviations used are: AXE, acetylxylan esterase; SIRAS, single isomorphous replacement and anomalous scattering.

TABLE I
Data collection statistics

Resolution range	Total observations	Unique reflections	Percent possible measured overall	Percent measured in last shell (0.94–0.90Å)	Intensity to S.D. ratio overall	Intensity to S.D. ratio in last shell	R_{merge} (last shell)
Å			%				
99.00–0.90	420,882	95,343	86.6	40.4	29.2	5.5	0.058 (0.185)

finement followed by simulated annealing starting at 3000 K. Individual atomic temperature factors were refined isotropically yielding an R factor of 0.333. The refinement was further continued with SHELX97. Twelve cycles of conjugate gradient least squares minimization using SHELX97 were carried out leading to a convergence. A test data set of 5% of the total was used for calculating R_{free}. During first six cycles, the model was refined isotropically and 290 fully occupied solvent waters and 3 sulfate ions were included in the model. Multiple conformers of serines 31, 36, 50, 58, 70, 74, 90, 120, 204 and tyrosine 177 were also included in the model. At this stage of the refinement, the R factor was 0.154 with an R_{free} of 0.169. The seventh cycle of minimization included modeling of the disorder of Ser[160], Ser[196], and Gln[154] side chains. The following cycles of anisotropic refinement of all non-hydrogen atoms reduced the R factor by 0.04 and R_{free} by 0.035. Modeling of the multiple occupancies of His[187] and further addition of solvent led to the convergence of the refinement process at an R factor of 0.107 for all data. All the computer graphics work was performed on a Silicon Graphics Indigo2 workstation running CHAIN (18). A summary of refinement results is provided in Table II.

In contrast to other high resolution structures in which there were small regions of disorder (19, 20), neither the 295 K nor the 85 K structure of AXEII shows any weak or poorly defined electron density usually associated with dynamic disorder. The difference between the low and high temperature structures appears to be in the number of amino acid side chains with multiple conformations. The 85 K structure has more multiply observed side chains. However, this could also result from better modeling of side-chain conformations owing to better data quality and higher resolution. The low temperature structure also shows more ordered solvent molecules, with higher number of tightly bound water oxygens and sulfate ions, including the sulfate at the active site, which is absent in the 295 K structure.

RESULTS

Description of the Secondary and Tertiary Structure—The crystal structure of AXEII and the catalytic triad Ser[90]-His[187]-Asp[175] are shown in Fig. 1a. About 60% or 125 of its 207 amino acids are distributed in ten β-strands (β1 to β10) and six α-helices (α1 to α6). The remaining 82 residues are distributed in five type 1 and 2 β-turns, one γ-hairpin turn, and five extended loop regions. Fig. 1b is a schematic showing the topology of the secondary structure of AXEII. The strands, loops, and helices have been numbered based on their sequence of occurrence in the polypeptide. All ten cysteine residues are involved in five intrachain disulfide bridge formation (Cys[2]-Cys[79], Cys[46]-Cys[55], Cys[101]-Cys[161], Cys[147]-Cys[179], and Cys[171]-Cys[178]). These disulfide bridges involve at least one cysteine in the loop regions. The tertiary structure consists of a doubly wound α/β sandwich, having a central parallel β-sheet flanked by two parallel α- helices on each side. The catalytic cleft is located at the C-terminal end of the β-sheet near the center, bordered by helical residues 183–193 from one side and the loop 105–113 containing an anti-parallel pair of strands from the other. The geometry and relative orientations of side chains of the catalytic triad are similar to those previously observed in other members of the α/β hydrolase family, such as in cholesterol esterase (21).

The N terminus of the polypeptide chain is anchored at the second residue by a disulfide bond and then flows into a long strand, β1. The C-terminal end of β1 is adjacent to the catalytic serine at the active site. The polypeptide chain then describes a loop structure, loop 1 (λ1) between residues 13 and 20, before entering the helix α1. After completing the terminal strand β2

TABLE II
Refinement statistics

Protein atoms in the model	1442
No. of protein residues with multiple conformations	13
Solvent sulfates	4
Solvent waters	300
Solvent glycerols	4
Resolution range (Å)	99.0–0.90
Unique data used ($F > 0$)	95,283
Overall completeness (%)	86.6
Weighted R^2	0.276
Crystallographic R	
All data	0.107
$F > 4\sigma F$	0.103
R_{free}	
All data	0.132
$F > 4\sigma F$	0.128
Goodness of fit	2.46
Restrained goodness of fit	2.28
r.m.s. deviations	
Bond distance (Å)	0.016
Bond angle (°)	1.982
Dihedral angle (°)	25.230
Planarity (°)	1.717
Ramachandran plot statistics % of 168 residues excluding glycines and prolines in the most favored region	91.1

of the central β-sheet via a right-handed βαβ-crossover, the polypeptide chain forms a long loop, λ2, between residues 41 and 55, the conformation of which is stabilized by an intra-loop disulfide between Cys[46] and Cys[52]. The helix, α2, the longest secondary element in AXEII, comprises residues 56 through 79. The C-terminal Cys[79] of α2 is involved in the disulfide bridge with Cys[2], which anchors the N terminus. β3, having residues 83–89, is the central strand at the C-terminal end of which resides the catalytic Ser[90] residue. The backbone conformation of Ser[90] belongs to the very restrictive (+,−) quadrant of the Ramachandran plot, but otherwise is normal for a catalytic serine in esterases and lipases (22). β3 turns sharply into α3, a three-turn helix, which is the only helix in the interior of the molecule, surrounded completely by protein atoms. The C-terminal Cys[101] of the helix is disulfide-bridged to Cys[161] from loop λ5. This is followed by a 17-residue loop λ3 between 101 and 117, containing a short anti-parallel segment formed by β4 and β5. The loop ends in a two-turn helix α4 oriented nearly perpendicularly to the sheet, unlike other helices. The next segment of the polypeptide chain between residues 126 and 171 contributes three strands β6, β8, and β10 with terminal residues 127–131, 142–145, and 167–171, respectively, to the central β-sheet, as well as to a short anti-parallel segment, β7 and β9, consisting of residues 135–138 and 148–151, respectively, away from the sheet. The intervening loop λ4, the longest loop in the structure between residues 152 and 166, is held in place by a disulfide bridge between Cys[161] and Cys[101] from the C-terminal end of α4. All of the secondary structure crossovers
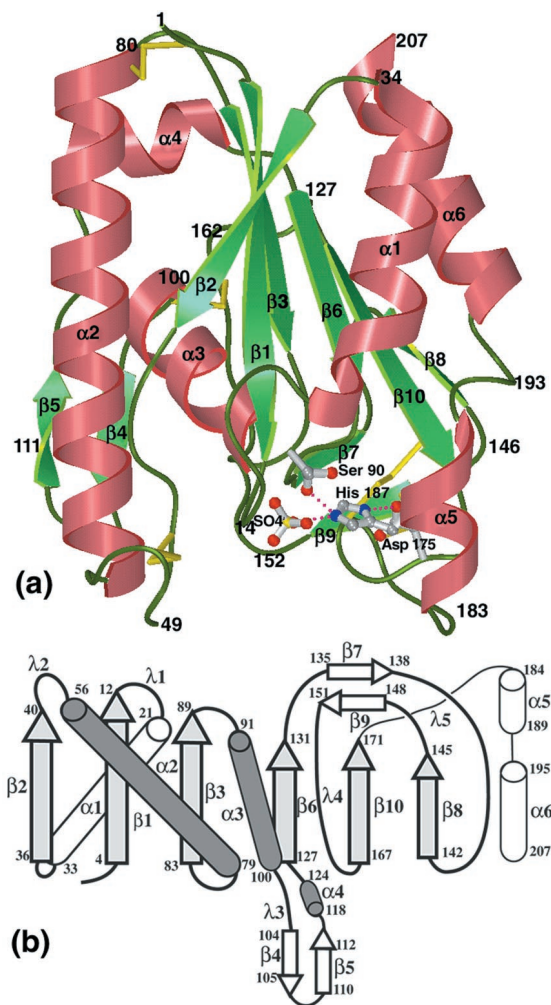
FIG. 1. *a*, a ribbon diagram of AXEII as determined at 85 K and 0.90-Å resolution. The secondary structures are *labeled* and *color-coded*. The catalytic residues and a bound sulfate ion are shown at the active site. Carbon atoms are shown in *gray*, nitrogen in *blue*, oxygen in *red*, and sulfur in *yellow*. Disulfide bonds are also shown in *yellow*. For clarity, His[187] side chain is shown only in the A state (see text for details) (drawn by SETOR (23)). *b*, a schematic diagram of the topology of AXEII and distribution of the secondary structure elements. α and β denote helices and strands while λ denotes loops. The N and C termini of secondary structure elements are *numbered*. *Open cylinders* represent helices below the central β-sheet, and *shaded cylinders* represent the ones above.

are right-handed, whereas the β8-loop-β10 crossover is left-handed. This segment of the polypeptide consisting of peripheral strands and loops are held together by two additional disulfide bonds, between Cys[147] and Cys[179], and between Cys[171] and Cys[178], which also anchor the next loop, λ5 consisting of residues 172–183. Asp[175] is contributed by this loop to the catalytic triad. Held by two disulfide bonds, the polypeptide chain makes a right-handed turn into a short helix α5 (residues 184–189), which contributes the last of the catalytic side chains, His[187]. This helix is separated from the C-terminal helix α6 (residues 195–207) by five intervening residues.

Comparison with Fusarium solani Cutinase—The only other known structure that is similar to AXEII is that of cutinase, an esterase that hydrolyzes cutin, a polyester component of the waxy layer of a plant's cuticle. The structure of cutinase has been determined at 1.0-Å resolution (20). Fig. 2 shows a super-position of backbones of AXEII and cutinase. Table III is an alignment of the AXEII amino acid sequence (7) with that of cutinase based on the secondary structures. In comparison with AXEII, cutinase has 29 additional residues at the N terminus of which the first 16 belong to a signal peptide. The next 13 are present in the crystal structure, where residues are numbered from 17 to 213 (197 amino acids; Protein Data Bank code: 1CEX). Although the overall similarity between the two tertiary structures is striking (the root mean squared deviation for 170 Cα atoms is ~1.2Å), long insertions and deletions, substitutions, and altered disulfide bond structure account for a large number of local conformational changes, especially in loops around the active site. AXEII has five disulfide bonds, whereas cutinase has only four of these cysteines bonded into two disulfides. All three of these additional disulfides (Cys[46]-Cys[55], Cys[101]-Cys[161], and Cys[147]-Cys[179]) are involved in anchoring loops surrounding the active site that are associated with large conformational differences between two polypeptides. In contrast, loop λ1 (residues 13–21) between α1 and β1, adjacent to the active site but away from the substrate-binding cleft, is conformationally quite similar to the one in cutinase. The conformations of λ2 (residues 41–55) in these two structures are such that they project in opposite directions: in cutinase more toward the interior, in the direction of the active site, whereas in AXEII it is pulled outward away from the active site by the disulfide bridge between Cys[46] and Cys[52]. A conformation of this loop like the one in cutinase would be in direct steric conflict with λ3 absent in cutinase. Also, the region 41–43 of the loop has a deletion of three residues in comparison with cutinase, which shortens the path to the disulfide bridge.

FIG. 2. **Superposition of backbones of AXEII (*green*) and cutinase (*pink*), shown roughly in the same orientation as in Fig. 1*a*.** Disulfide bonds are shown in *yellow*.
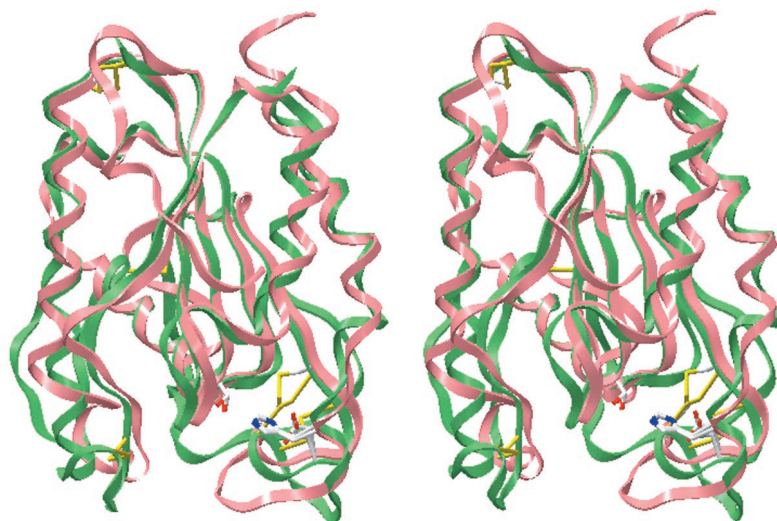
TABLE III
Sequence alignment of AXEII and cutinase based on three-dimensional structures

Element	β	α	Loop	β	Loop	α	β	Loop	α	β	α	β
Cutinase	18–21	22–26	27–32	33–42	43–51	52–63	67–73	74–89	90–109	113–119 Ser^{120}	121–131	
Axe				4–12	13–20	21–33	36–40	41–55	56–79	83–89 Ser^{90}	91–100	104–105

Element	β	α	β	β	β	β	Loop	β	Loop	α	Loop	α
Cutinase		135–140	142–148	(loop149–165)			166–172	173-Asp^{175}–184	185-His^{188}–190			192–212
Axe	110–112	118–124	127–131	135–138	142–145	148–151	152–166	167–171	172-Asp^{175}–183	184-His^{187}–189	190–194	195–207

FIG. 3. **A view of the catalytic triad in A and B states.** Carbon atoms are shown in *gray*, nitrogen in *blue*, oxygen in *red*, and sulfur in *yellow*. *Gray bonds* depict the A and *green* the B states. Bonds that belong to both states are also shown in *gray*. The electron density shown is from a final ($2F_{obs} - F_{calc}$) map, contoured at 1.8σ. The view is oblique to the imidazole ring of His^{187}.
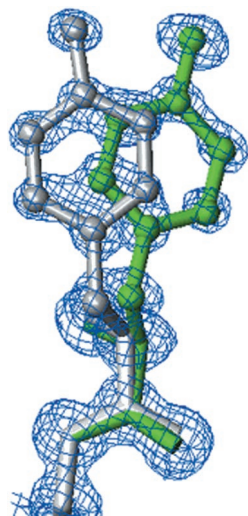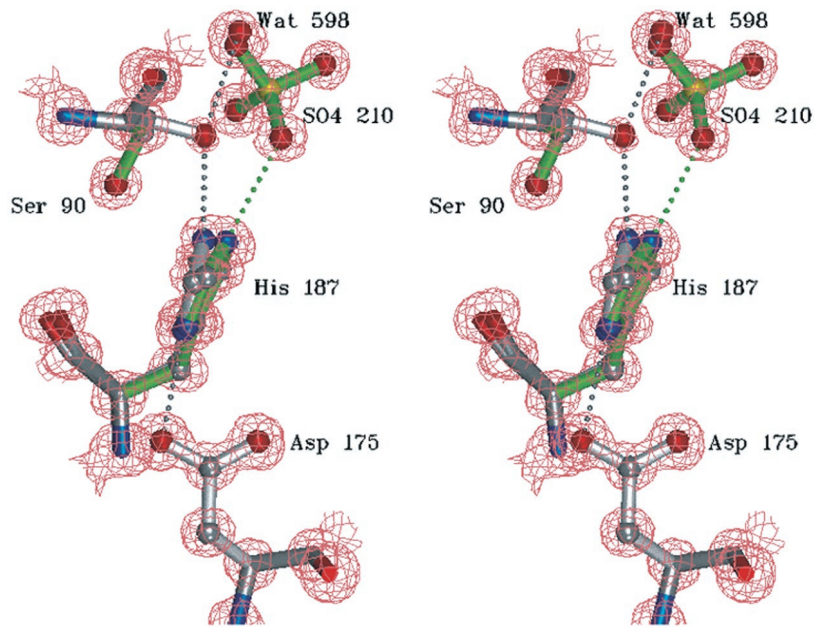
FIG. 4. **Movement of Tyr^{177} from A (*gray*) to B (*green*) states.** The electron density is from a final ($2F_{obs} - F_{calc}$) map, contoured at 1.0σ.

The loop λ3 consists of an insertion of residues 101–115 that contain a short anti-parallel segment (β4–β5). This segment of polypeptide is absent in cutinase. Its strategic positioning at the rear wall of the active site opening suggests its distinctive role in recognition and processing of acetate side groups of a chain of D-xylopyranose as opposed to cutin molecules by cutinase. The next major difference between the two structures is in loop regions, including λ4, which spans between residues 148 and 166 for cutinase, corresponding to residues 132 and 166, respectively, in AXEII, in spatial positions. This 16-residue insertion in this segment is distributed mainly between two short anti-parallel strands β7 (135–138) and β9 (148–151), and the sixth strand of the central β-sheet, β8. Not one of these features of the region is present in cutinase. The presence of Cys^{101}-Cys^{161} disulfide in AXEII also drastically alters the course of the backbone between residues 154 and 166, although these residues in the two proteins are analogous to each other in spatial positions and sequence alignment. The loop λ5 (residues 172–183 in AXEII and 172–184 in cutinase) contributes Asp^{175} to the catalytic triad and has one conserved disulfide (Cys^{171}-Cys^{178}); however, the additional disulfide in AXEII (Cys^{147}-Cys^{179}) alters the course of the main chain by pulling it away from the catalytic cleft. In addition to one residue insertion between 179 and 184, the backbone of cutinase in this segment adopts a different path such that the distance between Cα positions of 181 in AXEII and the equivalent 182 in cutinase is 10.4Å. This altered conformation of the polypeptide chain in cutinase partially shields catalytic Asp^{175} and His^{188} from exposure to the solvent, in contrast to exposed catalytic His^{187} in AXEII. Besides, a cutinase-like path for this segment of λ5 in AXEII would put residues 178 and 179 in steric conflict with the backbone of 150–152 of λ4. Residue 184 marks the beginning of a two-turn helix α5, which contains the catalytic histidine (His^{187} and His^{188}, in AXEII and cutinase, respectively) and is quite similar in both structures. The C-terminal helix α6 in AXEII is similar to that in cutinase, except for the fact that cutinase has four additional C-terminal residues in the helix.

The secondary structure elements of the two proteins are otherwise quite similar, except for occasional insertion or deletion of few residues and their spatial displacement. The β-sheet core of the two structures superimposes almost perfectly, except for the terminal strand β2 and the missing β8 in cutinase. The Cα positions and side-chain atoms of the catalytic residues superimpose with an average deviation of 0.3 Å from each other.
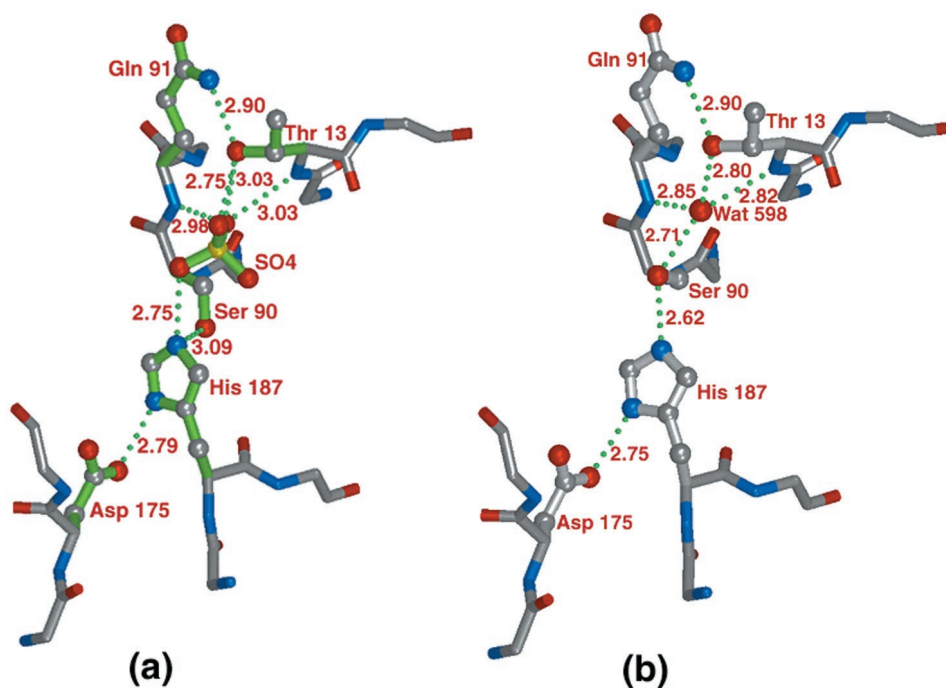
FIG. 5. **Hydrogen bonding interactions at the active site of AXEII in (*a*) B states and (*b*) A state.** Side chains of residues Ser[90], His[187], Asp[175], Thr[13], and Gln[91] in both states, as well as SO4 210 and water 598 in B and A states, respectively, are shown. Carbon atoms are shown in *gray*, nitrogen in *blue*, oxygen in *red*, and sulfur in *yellow*. Bonds in the B state are shown in *green*.

FIG. 6. **Docking of 2-acetyl xylopyranose in the active site of AXEII.** Side chains shown are Ser[90], His[187], Asp[175], Glu[12], Thr[13], Tyr[57], Gln[91], Phe[152], Tyr[177], and Gln[188]. Carbon atoms are shown in *gray*, nitrogen in *blue*, and oxygen in *red*. Disulfide bonds are shown in *yellow*. In this orientation Ser[90] Oγ is roughly normal to the acetate plane at a distance of 2.6 Å to the carbon atom.
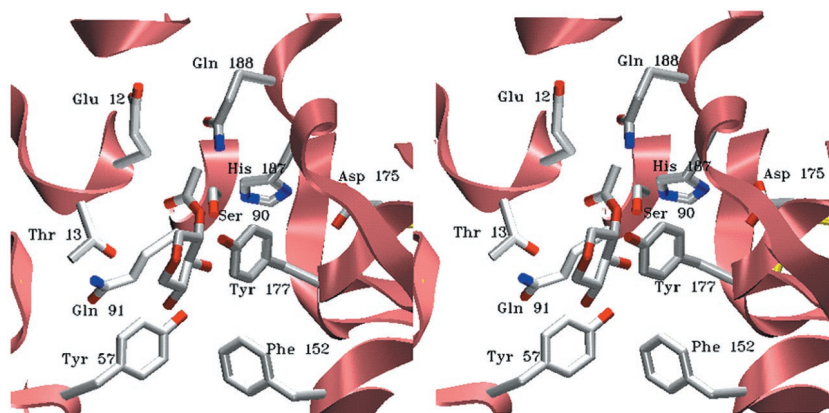
The Active Site and Multiple Conformations of Catalytic Residues—The active site gorge (Fig. 1*a*) is bordered by the following segments of the tertiary structure: λ1 (residues 13–20) and λ2 (residues 41–55) to the *left*, in the view in Fig. 1*a*; β3-to-α3 turn at the center of the gorge, where the three side chains of the catalytic residues are located; and, helix α5, λ5 (residues 175–183), β6-to-β7 turn (residues 132–134), and λ4 (residues 152–161) to the *right*. The opening of the active site is ~11 Å across, 7 Å thick from the surface to the catalytic triad, and has a depth of 20 Å to the back wall delineated by residues of λ3 (101–117). Residues lining the gorge are Glu[12], Tyr[89], Ser[21], Thr[24], Gly[191], Tyr[190], Thr[186], Pro[176], Tyr[177], Gln[188], Thr[13], Thr[14], Gln[49], Gly[47], Tyr[57], Pro[134], and Phe[152]. A sulfate ion, a glycerol, and about 40 water molecules fill up the entire cleft.

Of the catalytic residues, Ser[90] and His[187] side chains are fairly exposed to the solvent (each generating 7.1 and 5.7 Å^2 of solvent-accessible surfaces, respectively). In contrast, Asp[175] is shielded from the solvent by the helix α5 and Pro[176]. Fig. 3 depicts the two conformations of the catalytic residues observed in the 0.90-Å crystal structure determined at 85 K. The *gray* and *green* side chains of Ser[90] and His[187] represent conformations A and B, corresponding to 40 and 60% of the mol-

ecules in the crystal, respectively. In the A conformation, the most commonly observed in the resting state of esterases and lipases, as well as in the 295 K structure of AXEII (12), Ser[90] side chain is *trans* (χ$_1$ = −172°), whereas the Ser[90] Oγ and Asp[175] Oδ1 atoms are in the plane of the imidazole ring of His[187] (deviations of these two atoms from the plane are 0.03 and 0.02 Å, respectively; root mean square deviation from planarity of the ring is 0.05 Å). In the B conformation, the Ser[90] side chain is *gauche* (χ$_1$ = −65°) and the Oγ . . . Nε2 His[187] distance is 3.09 Å, at an approach angle of 102° to the imidazole ring. The two His[187] conformations have an average deviation of 0.40 Å with a maximum of 0.80 Å between two Nε2 atoms. The (φ,ψ) angles of His[187] A and B conformers are (−62°, −30°) and (−60°, −20°), respectively, and, side-chain (χ$_1$, χ$_2$) torsion angles are (−164°, 61°) and (−164°, 51°), respectively.

Conformational states A and B for the catalytic Ser[90] and His[187] exist at averages of 40 and 60%, respectively, of the volume of the crystal. The A state is not significantly different from the 1.10-Å structure at 295 K (12). A to B transition necessitates some rearrangement of other residues of the active site as well. The most notable of them is the movement of Tyr[177], which is at a van der Waal's contact distance from the
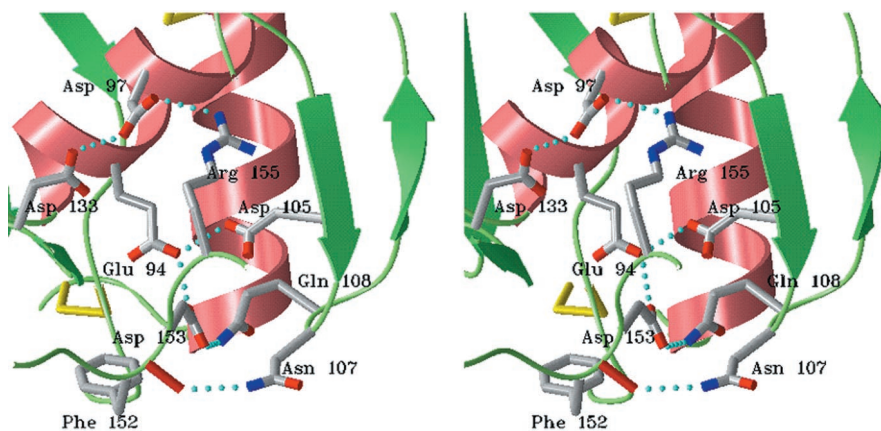
FIG. 7. **Hydrogen bond formation by the anti-parallel loop λ3.** Other interactions among charged side chains in the area are also shown. Carbon atoms are shown in *gray*, nitrogen in *blue*, and oxygen in *red*. Disulfide bonds are shown in *yellow*.
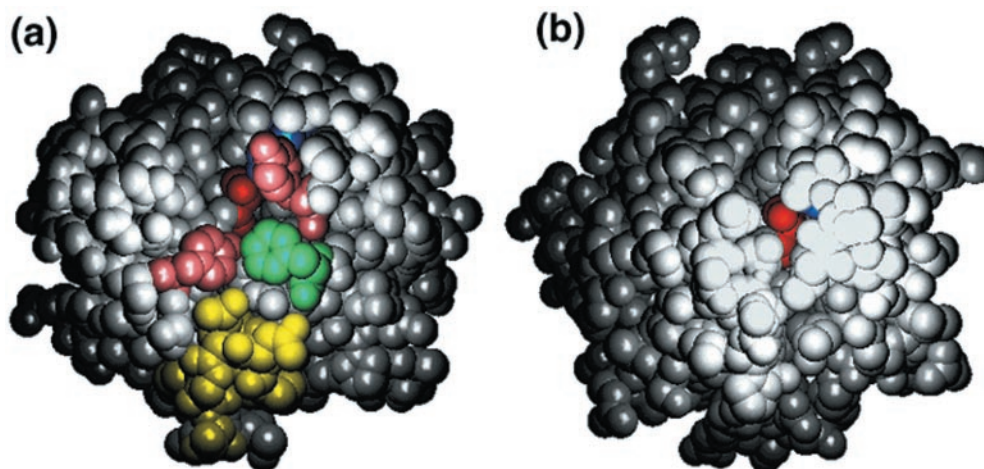

FIG. 8. **Space-filling models of (*a*) AXEII and (*b*) cutinase, viewed directly into the active site gorge from bottom in Fig. 1*a* (or Fig. 2).** Catalytic Ser and His are shown in *red* and *blue*, respectively. The Asp of the triad is not visible. In *a*, Tyr[177] and Tyr[57] are shown in *pink*, Phe[152] in *green*, and residues of the anti-parallel loop λ3 in *yellow*.

His[187] side chain in the A state. Tyr[177] moves about 2 Å away to accommodate His[187] in the B state (Fig. 4). The transition to the B state at 85 K could have been initiated by binding of a sulfate ion to the His[187] Nε2 atom through a hydrogen bond formation (His[187] Nε2 . . . O2 SO4 210: 2.75Å) (Fig. 5*a*). O2 of SO4 210 is also hydrogen-bonded (2.75 Å) to water oxygen 473, which, in turn, forms a hydrogen bond with Tyr[57] side-chain hydroxyl (2.89 Å). The sulfate ion makes four additional hydrogen bond-forming contacts with protein atoms as shown in Fig. 5*a*: O3 to Thr[13] Oγ (3.03 Å), to Thr[13] backbone NH (3.03 Å), and to Gln[91] backbone NH (2.98 Å), and O4 to Thr[13] Oγ (2.75 Å). In addition, the O1 oxygen of sulfate is coordinated to three water oxygens 465, 488, and 489 through strong hydrogen bonds (average distance ~2.80 Å) in a tetrahedral manner, all of which are linked to protein atoms by hydrogen bonds (to Gln[188] Nε2, Thr[13] backbone carbonyl, and Ser[90] Oγ; average distance ~2.84 Å). In the B state, binding of the sulfate ion eliminates three water oxygens that are present only in the A state, namely, 598, 599, and 600. O3 of the sulfate ion replaces water oxygen 598. However, binding of the sulfate ion does not affect water oxygens 465, 473, 488, and 489, all of which are strongly coordinated to protein atoms. These water molecules are also present in the 295 K structure. There is an estimated net gain of two hydrogen bonds in the transition from the A state to the B state.

An oxyanion binding site is comprised of two backbone amide groups of Thr[13] and Gln[91], as well as Ser[90] Oγ and Thr[13] Oγ hydroxyls in the A state, as shown in Fig. 5*b*. The Thr[13] side

chain is stabilized by a hydrogen bond from Gln[91] Nε2 (2.90 Å). The water oxygen 598 is thus bound at this oxyanion binding site in a roughly tetrahedral geometry. In the B state, SO4 210 occupies the oxyanion hole by replacing water 598; the position of O3 of the sulfate nearly coincides with the oxygen atom of water 598. Furthermore, in the B state, O2 of SO4 210 occupies what used to be the Ser[90] Oγ position relative to the His[187] imidazole ring in the A state, thus maintaining an orientation to the imidazole ring similar to that of Oγ in the A state.

Other Residues in Alternate Conformations—In addition to Ser[90], Tyr[177], and His[187], 10 serine (residues 31, 36, 50, 58, 70, 74, 120, 160, 196, and 204) and Gln[154] side chains possess two alternate conformations. These were identified from positive and negative difference electron density maps. The occupancies of the major conformations range between 55 and 75%. All of the alternate conformers have hydrogen bond-forming partners, either protein or solvent atoms, in both conformations. Side chains of the rest of the amino acid residues have well characterized electron densities that uniquely define their conformations. Unlike other high resolution structures, no dynamically disordered region of the polypeptide chain is identifiable. Only the residues at two termini have significantly higher than average temperature factors; their average equivalent isotropic temperature factors are 25 and 45 Å² for main-chain and side-chain atoms, respectively. The average equivalent isotropic temperature factor for the rest of the protein C, N, and O atoms is about 12 Å².

Packing Interactions in the Crystal—One of the closest pack-

ing interactions between secondary structure elements in the crystal occurs between $\alpha 1$ of one molecule and $\alpha 2$ of another. However, very little direct hydrophobic packing surfaces are involved in these close contacts. Instead, several solvent molecule-mediated interactions dominate this molecular interface. Notable among these include a sulfate ion (213)-mediated contacts between Thr[24] Oγ of $\alpha 1$ and Asn[73] N$\delta 2$ and Ser[70] Oγ of $\alpha 2$. Several water molecules line this interface. The closest approach between the helices is at Ala[62] Cβ of $\alpha 2$, which is at a van der Waal's contact distance (3.84 Å) from Ser[31] Cα of $\alpha 1$. In the second conformation, Ser[31] Oγ also makes a water-mediated (449) contact to OH of Tyr[110] of $\beta 5$ of the same neighboring molecule. The backbone amide of N-terminal Gly[35] of $\alpha 1$ donates the proton to the backbone carbonyl oxygen of Gly[109] from $\beta 5$, thereby forming an intermolecular hydrogen bond. A second intermolecular hydrogen bond is formed in this region between the backbone carbonyl of Ser[36] from $\beta 2$ and Thr[111] Oγ. In addition, the C-terminal end of $\alpha 2$ is involved in two intermolecular hydrogen bonds: Ser[77] backbone carbonyl to Asn[180] side chain and Gln[78] side chain to Gly[48] backbone carbonyl. Gln[78] N$\epsilon 2$ also accepts a proton from an alternate conformation of Ser[50] Oγ across the molecular interface. Asn[180], Ser[50], and Gly[48] are all from extended loop regions of the molecule. Gly[53] Cα from the disulfide stabilized loop $\lambda 2$ packs (3.83 Å) against Ala[149] Cα, from the adjacent molecule. Other short contacts in this loop-loop interaction between two molecules include an approach (3.07 Å) of Asn[42] backbone carbonyl oxygen to Gly[139] Cα and packing of Pro[17] side chain against Thr[146] Cα.

Intermolecular hydrogen bond formation between two alternate conformations of serine Oγ atoms is also observed at the packing contact between the N terminus of helix $\alpha 6$ and the loop $\lambda 4$ region (residues 159–161) of a neighboring molecule. In one conformation, Ser[196] side chain forms a hydrogen bond to an alternate conformation of Ser[160] Oγ and in its second conformation, the hydrogen bond is formed between the side chain and the backbone amide of Ser[160]. Again, several water molecules tightly hydrogen bonded to protein atoms are found at this interface. The other two direct intermolecular contacts between these two regions involve a hydrogen bond between Lys[203] side chain of $\alpha 6$ and Gly[157] backbone carbonyl, and the packing of Leu[199] C$\delta 2$ against Gly[158] Cα (4.16 Å). Although the C terminus approaches the anti-parallel loop $\lambda 3$, there is no direct contact between the two. Intermolecular contacts in this region involve interactions between Lys[83] side chain and backbone carbonyl of Asn[107], and between Ala[81] backbone carbonyl and Asn[107] side chain.

A packing interaction that involves nonpolar contacts occurs in the region where the short helix $\alpha 4$ approaches $\lambda 4$ after $\beta 9$. Met[124] Sδ from $\alpha 4$ has a van der Waal's contact (3.75 Å) with Phe[152] Cβ of the adjacent molecule. In the same region, the carbonyl oxygen of Pro[80] has a short contact (3.25 Å) to Cα of Phe[152]. Ser[120] side chain from $\alpha 4$, in its more occupied conformation, approaches the loop $\lambda 5$ that contributes Asp[175] to the catalytic triad, by donating the proton to the Pro[176] backbone carbonyl oxygen. In addition, side chains of residues Asn[183] and Ala[185], near the N terminus of $\alpha 5$ packs against side chains of Thr[14] and Ala[15] from $\lambda 1$ and Ser[51] from $\lambda 2$, respectively, of a symmetry-related molecule. The crystal packing of AXEII is, thus, dominated by polar interactions; there are only a few interactions among hydrophobic side chains.

DISCUSSION

The Active Site and Possible Binding Modes of the Substrate—Coexistence of two different conformational states, perhaps representing two oxidation states of catalytic Ser and His residues in the same crystal, is a major finding that was only possible due to extraordinarily high resolution of the study. In the state A, which is the resting state of the enzyme resembling the geometry of the side chains in the 295 K structure (12), it is likely that Ser[90] OγH is the proton donor in the Ser[90] OγH ... N$\epsilon 2$ His[187] hydrogen bond. It was shown for cutinase that N$\epsilon 2$ is deprotonated (19). In the presence of a negatively charged sulfate ion, which is a strong nucleophile and makes a direct contact (2.75 Å) to His[187] N$\epsilon 2$, it is likely that N$\epsilon 2$ retains the proton due to increase in pK_a. (Efforts to locate this proton from the difference electron density maps were unsuccessful, perhaps due to complications from modeling the side chain in two alternate conformations.) The B state, therefore, could be a mimic of the binding of the tetrahedral intermediate to His in which the imidazole ring has an overall positive charge. Although the Ser side chain in the B state assumes a catalytically "inactive" position, the proximity and orientation of the Ser Oγ proton to the N$\epsilon 2$ of His[187] could contribute to the stability of the B state. The movement of residues His[187] and Tyr[177], demonstrated by multiple conformations of their backbone and side-chain atoms, is perhaps reflective of the motion within the catalytic cavity during intermediate steps of catalysis.

In an attempt to comprehend substrate-protein interactions, a 2-acetyl xylopyranose molecule, a substrate for AXEII (3), was manually docked at the active site in one of at least two possible orientations of the pyranose ring (Fig. 6). In this position, Ser Oγ is oriented roughly normal to the acetate plane at a distance of 2.6 Å to the carbon atom. In both orientations, however, the pyranose ring stacks against the Tyr[177] side chain. Interestingly, the location of the pyranose ring nearly coincides with the only glycerol molecule found in the active site. In this binding mode, the acetate group is at a van der Waal's contact distance from the backbone and side-chain atoms lining the pocket, namely Thr[13] NH and His[187] CO and side-chain atoms of His[187], Glu[12], Tyr[89], and Gln[188]. The acetate group thus fits nicely in this pocket, which seems to be tailored to accommodate such a moiety. This observation is consistent with the biochemical data that AXE II has high specificity for the acetate ester and only weakly hydrolyzes esters of longer fatty acids (3). Alternatively, a small substrate like 2-acetyl xylopyranose may flip around and bind in a direction opposite to the one shown in Fig. 6. The acetyl group would then face the longer end of the active site, thus making room for longer fatty acid side chains to bind and be hydrolyzed. However, in this mode the xylopyranose moiety binds to the interior of the molecule, precluding the possibility of a polymeric substrate such as an acetylated xylan from binding at the active site.

Other residues that the substrate may have direct contact with are Tyr[57], Gln[91], and Phe[152] (Fig. 6). In the active site gorge, which is about 20 Å long to the back wall containing the anti-parallel loop $\lambda 3$ (see the description of the active site in the result section), an estimated four to five xylose residues of a xylan chain could be accommodated. If a xylan chain binds at the active site, then xylose residues may additionally make contacts with residues Ser[58], Asp[153], Glu[158], and Asn[107].

It is possible that the loop $\lambda 3$ containing the anti-parallel strand $\beta 4$–$\beta 5$ plays a special role in recognition and binding of a xylan chain. This loop, absent in cutinase, is nearly 10 Å away from the substrate atoms when a single molecule of xylose binds at the active site (Figs. 7 and 8). However, it may serve as a gate to the active site for binding of a xylan chain. Interestingly, the loop is loosely anchored to the rest of the molecule by hydrogen bonds near the turn, Gln[108] N$\epsilon 2$ ... O$\delta 1$ Asp[153] (2.92 Å), Asn[107] N$\delta 2$ ... OC Phe[152] (2.99 Å), and Asp[105] O$\delta 1$ ... O$\epsilon 1$ Glu[94] (2.54 Å). There are several acidic side chains in this region that are linked to each other by hydrogen bonds, as shown in Fig. 7. These residues are, therefore, protonated at the

crystallization pH of 5.3. Deprotonation of these residues, coupled with conformational changes, could trigger breakage of the hydrogen bonds and release of the loop. This structural flexibility could be critical to its role as the "gatekeeper" of the active site gorge and recognition of a xylan chain.

Accessibility of the Active Site—As described under "Results" and in the discussion above, the active site gorge of AXEII is more exposed than the only other known structure of the same family, cutinase. With a water molecule as the probe, the accessibility surface for the catalytic Ser and His is more for AXEII (12.8 Å^2) than for cutinase (7.9 Å^2). In contrast, catalytic residues are relatively buried in cutinase, as has been illustrated in Fig. 8. Not only the Ser[90] and His[187] side chains are more exposed, but also the gorge stretches wider in AXEII than in cutinase. A few side chains, such as Tyr[177], Tyr[57], and Phe[152] cover the gorge, as shown in Fig. 8, reducing its accessibility. Furthermore, the gatekeeper loop limits the access to the gorge for the xylan chain. However, as has been pointed out, some of these residues and the loop belong to flexible regions of the molecule, and it is likely that they undergo movement to accommodate a xylan chain. The openness of the active site is suggestive that AXEII is a "pure" esterase as opposed to a lipase that functions as an esterase on esters of long-chain fatty acids or substrates containing lipid-like side groups. AXE II, in contrast, uses polar molecules as substrates, as an AXE should.

Molecular Packing—Despite the overall compact nature of the AXEII molecule, 82 of 207 residues are located in loops and turns. Although each of five disulfide bridges involves at least one Cys from loops and turns, three have both Cys residues belonging to extended loop regions of the molecule, namely λ2, λ3, λ4, and λ5. The internal rigidity of the AXEII molecule is a direct consequence of well-packed secondary structure elements and disulfide-stabilized loops and turns. Some of the loop regions are highly polar and form parts of the outer surface. The central theme in packing of AXEII molecules in the unit cell is: few hydrophobic and many polar interactions, the presence of interfacial solvent molecules and solvent-mediated protein-protein interactions, and strong loop-loop contacts in several extended loop regions. These are all characteristics of a tightly folded monomeric, soluble, globular protein. A high long range order of the crystal could, however, be a consequence of the molecule's overall shape and its highly polar surface property that is conducive to close packing. The overall shape of the molecule resembles a cylinder of an average diameter of 27 (±3) Å and a height of 38 (±3) Å. These cylindrical molecules are packed in the unit cell with the cylinder axes along the *z* axis, which, interestingly, is also roughly the direction along which major helices and the central β-sheet are aligned.

REFERENCES

1. Joselau, J. P., Comptat, J., and Ruel, K. (1992) *Prog. Biotechnol.* **7,** 1–15
2. Biely, P. (1985) *Trends Biotechnol.* **3,** 286–290
3. Egaña, L., Gutiérrez, R., Caputo, V., Peirano, A., Steiner, J., and Eyzaguirre, J. (1996) *Biotechnol. Appl. Biochem.* **24,** 33–39
4. Williamson, G., Kroon, P. A., and Faulds, C. B. (1998) *Microbiology* **144,** 2011–2023
5. Christov, L. P., and Prior, B. A. (1993) *Enzyme Microb. Technol.* **15,** 460–475
6. Wong, K. K. Y., and Saddler, J. N. (1993) in *Hemicellulose and Hemicellulases*, (Coughlan, M. P., and Hazlewood, G. P., eds) pp. 127–143, Portland Press, London
7. Gutiérrez, R., Cederlund, E., Hjelmquist, L., Peirano, A., Herrera, F., Ghosh, D., Duax, W., Jörnvall, H., and Eyzaguirre, J. (1998) *FEBS Lett.* **423,** 35–38
8. Biely, P., Puls, J., and Schneider, H. (1985) *FEBS Lett.* **186,** 80–84
9. Poutanen, K., and Sundberg, M. (1988) *Appl. Microbiol. Biotechnol.* **28,** 419–424
10. Margolles-Clark, E., Tenkanen, M., Söderlund, H., and Pentillä, M. (1996) *Eur. J. Biochem.* **237,** 553–560
11. Pangborn, W., Erman, M., Li, N., Burkhart, B. M., Pletnev, V. Z., Duax, W. L., Gutiérrez, R., Peirano, A., Eyzaguirre, J., Thiel, D. J., and Ghosh, D. (1996) *Proteins Struct. Funct. Genet.* **24,** 523–524
12. Ghosh, D., Erman, M., Sawicki, M., Lala, P., Weeks, D. R., Li, N., Pangborn, W., Thiel, D. J., Jörnvall, H., Gutiérrez, R.,, and Eyzaguirre, J. (1999) *Acta Crystallogr. Sect. D Biol. Crystallogr.* **55,** 779–784
13. Eyzaguirre, J and Ghosh, D. (1999) in *Recent Advances in Carbohydrate Bioengineering* (Gilbert, H. J., Davies, G. J., Henrissat, B., and Svensson, B., eds) 117–123, Special Publication No. 246 of the Royal Society of Chemistry, Cambridge, UK
14. Hakulinen, N., Tenkanen, M., and Rouvinen, J. (1998) *Acta Crystallogr. Sect. D Biol. Crystallogr.* **54,** 430–432
15. Otwinowski, Z., and Minor, W. (1995) in *The HKL Manual*, Yale University, New Haven, CT
16. Brünger, A. T. (1997) *X-PLOR Manual 3.8*, Yale University, New Haven, CT
17. Sheldrick, G. M. (1997) *The SHELX-97 Manual*, Göttingen University
18. Sack, J. S. (1988) *J. Mol. Graphics* **6,** 224–225
19. Teeter, M. M., Roe, S. M., and Heo, N. H. (1993) *J. Mol. Biol.* **229,** 419–427
20. Longhi, S., Czjzek, M., Lamzin, V., Nicolas, A., and Cambillau, C. (1997) *J. Mol. Biol.* **268,** 779–799
21. Ghosh, D., Wawrzak, Z., Pletnev, V., Li, N., Kaiser, R., Pangborn, W., Jörnvall, H., Erman, M., and Duax, W. L. (1995) *Structure* **3,** 279–288
22. Ollis, D. L., Cheah, E., Cygler, M., Dijkstra, B., Frolow, F., Franken, S. M., Harel, M., Remington, S. J., Silman, I., Shrag, J., Sussman, J. L., Verschueren, K. H. G., and Goldman, A. (1992) *Protein Eng.* **5,** 197–211
23. Evans, S. V. (1993) *J. Mol. Graphics* **11,** 134–138